ChemComm

COMMUNICATION

View Article Online
View Journal | View Issue

Cite this: *Chem. Commun.*, 2019, **55**, 12912

Received 4th September 2019,
Accepted 1st October 2019

DOI: 10.1039/c9cc06888k

rsc.li/chemcomm

Construction of a two-photon fluorescent probe for ratiometric imaging of hypochlorous acid in alcohol-induced liver injury†

Yan Lou,‡[a] Caixia Wang,‡[a] Siyu Chi,[b] Songjiao Li,[b] Zhiqiang Mao *[a] and Zhihong Liu *[ab]

Alcohol-induced liver injury has been a terrible threat to human health and life. The relationship between HClO and the process is unclear. Thus, a ratiometric two-photon fluorescent probe for HClO was deliberately constructed and revealed the generation of HClO in the alcohol-induced liver injury process for the first time.

Liver injuries caused by alcohol abuse, drug overuse and obesity have been a terrible threat to human health and life. Among them, alcohol-induced liver disease (ALD) is one of the most prevalent and lethal liver diseases in the whole world.[1] In the human body, most absorbed alcohol is metabolized in the liver through the alcohol dehydrogenase metabolic pathway, and heavy drinking generally imposes oppressive burdens on the liver's normal functions.[2] The chronic consumption of excessive alcohol in daily life can give rise to a broad spectrum of disorders, initializing liver injury and progressing alcoholic hepatitis, hepatocellular cancer and eventually liver failure. In the liver injury process, alcohol can trigger hepatic inflammation and the outburst of a massive amount of ROS, which exacerbate further liver damage.[3] Accordingly, studying the production and distribution of ROS in liver tissue is essential for revealing the function of ROS in the alcohol-induced liver injury process.

Among the ROS family, hypochlorous acid (HClO) is one of the utmost important endogenous ROS with potent oxidative capacity, which is produced by myeloperoxidase (MPO)-catalyzed peroxidation of chloride (Cl^-) and hydrogen peroxide in living systems.[4] It was discovered that HClO not only plays essential roles in regulating intracellular redox balance, but can also wipe out pathogens and microorganisms in the innate immune system and participate in several signalling processes.[5] Nonetheless, mounting evidence supports that superfluous HClO can result in oxidative stress in cells and organs, which is associated with various diseases and disorders, such as Parkinson's disease,[6] rheumatoid arthritis,[7] liver injuries,[8] and cancers.[9] Therefore, it's quite meaningful to develop a reliable and convenient method for investigating HClO in alcohol associated diseases.

To achieve this objective, plenty of one-photon (OP)/two-photon (TP) excited fluorescent probes for HClO have been exploited and reported in recent years.[10] Compared with one-photon probes, two-photon probes are more suitable for imaging of target analytes in tissues due to their larger imaging depths, longer observation times and higher signal-to-noise ratios.[11] Although these wonderful studies help in elucidating the role of HClO in a variety of biological processes, probing and monitoring HClO in alcohol-induced liver injury with fluorescent probes have not been reported yet perhaps due to the deficiency of response speed or sensitivity. Besides, to acquire more accurate information with fluorescent probes, ratiometric probes are more preferable due to their built-in self-calibration function, which can effectively eliminate the drawbacks of single emission-based probes, and thus give more reliable results.[12] Taking all the above into consideration, there is a keen desire to construct a ratiometric two-photon fluorescent probe for monitoring HClO in the alcohol-induced liver injury process.

To fabricate a ratiometric two-photon fluorescent probe for HClO, we adopted a triphenylamine derivative as a two-photon fluorophore due to its highly fluorescing and two-photon excitable properties.[13] Sulfur-containing compounds including thioketones, thioesters and thioethers usually can be efficiently and selectively oxidized by hypochlorite in buffer solutions according to previous reports.[14] Therefore, a triphenylamine moiety and a thioanisole moiety were elaborately coupled *via* a palladium-catalyzed Suzuki reaction to produce a new probe, **TPA-ClO** (Scheme S1 and Fig. S11–S13, ESI†). **TPA-ClO** features a D–π–D structure; on the other hand, after reacting with HClO, the thioanisole tends to be oxidized to a sulfoxide compound, forming a D–π–A structure. This would be beneficial for two-photon absorption and fluorescence properties due to the intramolecular charge transfer (ICT)

[a] *College of Chemistry and Chemical Engineering, Hubei University, Wuhan 430062, China. E-mail: maozq@hubu.edu.cn*
[b] *Key Laboratory of Analytical Chemistry for Biology and Medicine (Ministry of Education), College of Chemistry and Molecular Sciences, Wuhan University, Wuhan 430072, China. E-mail: zhhliu@whu.edu.cn*

† Electronic supplementary information (ESI) available. See DOI: 10.1039/c9cc06888k

‡ These authors contributed equally.

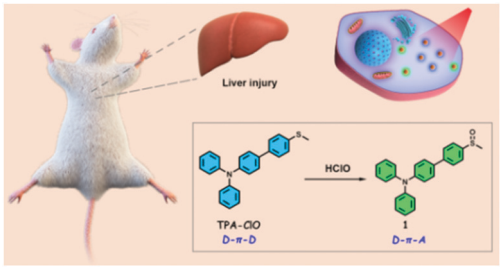

Scheme 1 Design of a ratiometric probe, **TPA-ClO**, for the detection of HClO in alcohol-induced liver injury.

effect (Scheme 1).[15] It was thus reasonably anticipated that the probe could provide ratiometric fluorescence signals for the precise *in vivo* detection of HClO in cells and animals.

To prove that the probes **TPA-ClO** with and without HClO were two-photon excitable, we examined the relationship between the excitation power of the laser and emission intensity. The slopes for the logarithmic plots (1.75 and 1.89) are close to 2.0, indicating the two-photon absorption process for both the probe and the reaction product (Fig. S1, ESI†). Next, to evaluate the feasibility of detecting HClO with **TPA-ClO**, the sensing performances of the probe toward HClO were first examined in PBS buffer solution. As shown in Fig. 1a and b, the probe shows a maximal UV absorption at 334 nm (ε = 2.0 × 10^4 M^{-1} cm^{-1}) and a strong fluorescence emission peaked at 437 nm (Φ = 0.32). After reacting with excessive HClO, the maximal absorption was shifted to 342 nm (ε = 2.1 × 10^4 M^{-1} cm^{-1}) and a new emission band emerged at 497 nm (Φ = 0.32). The remarkable changes in emission bands and high fluorescence quantum yields both before and after reacting with HClO indicated that the probe could detect HClO with a ratiometric fluorescence signal. Upon addition of an increasing amount of HClO, the ratio of the emission intensities at 497 nm and 437 nm (I_{497}/I_{437}) also increased drastically with a maximal ratio value of 3.6 (Fig. 1c). Notably, the emission ratio of **TPA-ClO** was found to be linear with HClO concentration in the ranges of 1.8–32 μM and 36–59 μM. And the limits of detection (LOD) were calculated to be 16 nM for HClO concentrations of 1.8–32 μM and 272 nM for HClO concentrations of 36–59 μM (Fig. S2 and S3, ESI†), which indicates that **TPA-ClO** exhibits a quite high sensitivity compared with previously reported HClO probes and is sensitive enough for detecting biological HClO levels. Furthermore, the reaction profile of **TPA-ClO** with HClO *versus* time was also examined. With excessive HClO, the ratio signal showed a significant increase within 40 s and then levelled off, suggesting the very high reactivity of **TPA-ClO** toward HClO (Fig. 1d). These results indicated the potential of **TPA-ClO** to sensitively determine HClO with high speed *in vitro*.

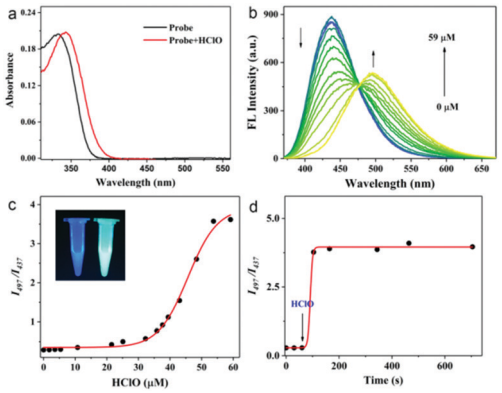

Fig. 1 (a) UV-vis absorption spectra of the probe **TPA-ClO** with and without excessive HClO. (b) Fluorescence spectra of 10 μM **TPA-ClO** in the presence of HClO (0–59 μM). (c) Plot of the fluorescence emission ratio (I_{497}/I_{437}) of **TPA-ClO** *versus* [HClO] (0–59 μM). Inset: Photograph of **TPA-ClO** before and after reacting with HClO under 365 nm excitation. (d) Time dependence of the fluorescence emission ratio (I_{497}/I_{437}) for 10 μM **TPA-ClO** in the presence of excessive HClO (60 μM). The measurements were carried out in PBS/DMF (v : v = 1 : 1, pH 7.4, 10 mM) solution. Reaction time: 60 s.

Next, the fluorescence responses of the probe toward HClO and other interfering species were checked. When **TPA-ClO** reacted with the other species including 20 μM metal ions (Cu^{2+}, Fe^{3+}, Hg^{2+}, Ca^{2+}, Mg^{2+}, Zn^{2+}, Fe^{2+}), 0.1 mM biothiols (Hcy, Cys and GSH), 20 μM ROS (H_2O_2, $^{\bullet}OH$, O_2^-) and 20 μM RNS (NO_2^-, $ONOO^-$, NO), no significant changes in the fluorescence ratio were observed (Fig. S4, ESI†). On the other hand, only HClO resulted in a significant increase of the ratiometric signal. Furthermore, the probe **TPA-ClO** was pH-insensitive in the pH range of 4.2–8.5, and the fluorescence ratio of the reaction product of **TPA-ClO** and HClO was also pH-insensitive in the neutral and weakly alkaline pH range (7.0–8.5), thus indicating that the probe is suitable for working in the physiological pH range (Fig. S5, ESI†). Therefore, it's safe to conclude that the probe can detect HClO in the complex cellular environment with a good selectivity.

To identify the reaction product, the reaction mixture of **TPA-ClO** and HClO was analyzed by HRMS. As expected, the molecular ion peak of the main product compound **1** ($[M + Na]^+$ = 406.1210) was found in the HRMS spectra (Fig. S6, ESI†), which evidently verified that **TPA-ClO** was transformed to sulphone derivative compound **1** and is in good agreement with the proposed reaction mechanism (Scheme 1).

To demonstrate the performance of **TPA-ClO** as a specific probe for HClO in live cells, two-photon imaging of exogenous and endogenous HClO in cells was carried out. Prior to cell imaging, the cytotoxicity of **TPA-ClO** was assessed by the MTT method, and the results clearly suggested its favourable biocompatibility, *i.e.*, the very low cytotoxicity of **TPA-ClO** toward HeLa cells even at a concentration as high as 40 μM (Fig. S7, ESI†). To detect exogenous HClO, HeLa cells were first incubated with **TPA-ClO** for 30 min, and then treated with various amounts of external HClO and measured under a two-photon microscope (TPM). As shown in Fig. 2a and d, the **TPA-ClO** stained cells showed moderate blue fluorescence and scant green fluorescence under the TPM. The results proved that the probe has a good cell membrane permeability and cellular retention ability. Upon addition of 20 μM HClO, a bright green fluorescence was observed, which can be ascribed to the fluorescence response of **TPA-ClO** to the adscititious HClO

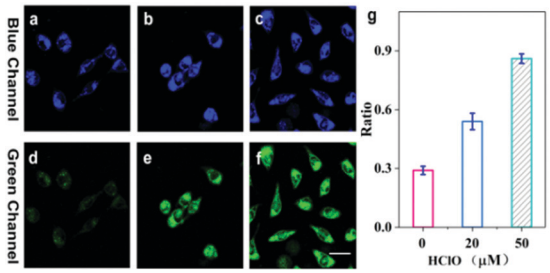

Fig. 2 Two-photon images of **TPA-ClO** in HeLa cells. HeLa cells were incubated with 10 μM **TPA-ClO** for 0.5 h (a and d), and then with 20 μM (b and e) and 50 μM HClO (c and f) for 0.5 h, respectively. (g) Fluorescence intensity ratios (F_{green}/F_{blue}) of a–f. The fluorescence intensities were collected in the blue channel (370–450 nm) and green channel (500–600 nm) upon excitation at 720 nm. Scale bar: 20 μm.

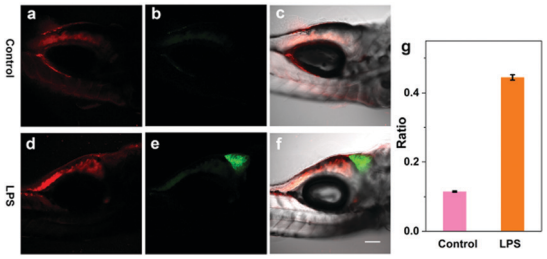

Fig. 3 *In vivo* visualization of endogenous HClO generation in zebrafish. 6-Day-old zebrafish was treated with 0 μg mL^{-1} (a–c) and 10 μg mL^{-1} (d–f) LPS for 2 h, and then incubated with 10 μM **TPA-ClO** for 1 h. (g) Fluorescence ratios of a–f. The fluorescence was collected at 370–480 nm (a and d) and 490–600 nm (b and e) upon excitation at 720 nm. Scale bar: 100 μm.

(Fig. 2b and e). Further, when **TPA-ClO** stained cells were incubated with 50 μM HClO, a much brighter green fluorescence and further decreased blue fluorescence were observed under the TPM (Fig. 2c and f). These results can also be quantitatively presented in terms of the fluorescence ratio of the green and blue emission channels (Fig. 2g). The remarkable changes in the fluorescence ratio manifested that the probe can sensitively detect exogenous HClO in live cells.

Encouraged by the excellent performances of the probe for exogenous HClO detection, we further tried to use the probe for the detection of endogenous HClO with a TPM. It's well documented that RAW264.7 mouse macrophages can generate excess HClO under the activation of phorbol-12-myristate-13-acetate (PMA), a well-known HClO stimulant.[16] Initially, **TPA-ClO** loaded RAW 264.7 cells exhibited a moderate blue fluorescence and extremely weak green fluorescence (Fig. S8a and d, ESI†). When the cells were pretreated with 500 ng mL^{-1} PMA, an enhanced green fluorescence was observed in cells, together with an increased ratio of green fluorescence to blue fluorescence (Fig. S8b and e, ESI†). Furthermore, when RAW 264.7 cells were pretreated with 500 ng mL^{-1} PMA and 0.5 mM NAC (*N*-acetyl-L-cysteine, a ROS scavenger), the fluorescence ratio of the green fluorescence to blue fluorescence was reduced (Fig. S8c, f and g, ESI†), which can be ascribed to the ROS scavenging ability of NAC and the reduced HClO level in cells. The above results convincingly elucidated that **TPA-ClO** is capable of detecting endogenous HClO in live cells.

The imaging depth of **TPA-ClO** under two-photon excitation in tissues *ex vivo* was then studied. Fresh mouse liver tissues were cultured with 50 μM **TPA-ClO** for 1 h, and then the tissues were imaged in *Z*-scan mode under excitation at 720 nm. The TP images clearly showed that **TPA-ClO** can stain the tissues evenly, and the morphology and structure of liver cells can be vividly observed in depths up to *ca.* 90 μm. These results evidenced that the probe can be used in deep tissue imaging under a TPM (Fig. S9, ESI†).

In the liver injury process, inflammatory cells are activated and subsequently cause inflammatory responses.[17] To confirm the outburst of HClO in this process, zebrafish larvae were selected as model organisms since they have conserved structures and immunity functions similar to mammals.[18] Previous reports have suggested that lipopolysaccharide (LPS) can induce acute liver injury in zebrafish and simultaneously spurs HClO production in the liver.[19] Thus, we further attempted to use the probe **TPA-ClO** to monitor HClO in the LPS-induced liver injury of zebrafish *in vivo* using a TPM. As a control, 6-day-old zebrafish was cultured with **TPA-ClO** for 2 h and then imaged. As shown in Fig. 3a, fluorescence at 370–480 nm was observed only in the intestines of the zebrafish, while there was almost no green fluorescence observed in the zebrafish (Fig. 3b and c). The imaging results demonstrated that **TPA-ClO** can stain the zebrafish intestines through the digestion process, and there was nearly no HClO production in the normal zebrafish liver (Fig. 3b and c). When the zebrafish was treated with 10 μg mL^{-1} LPS for 2 h, the liver area exhibited bright green fluorescence (Fig. 3e and f), and the intestines also displayed fluorescence (Fig. 3d). The above results suggested that **TPA-ClO** can selectively accumulate in the zebrafish liver and trace the increase of HClO in the LPS-induced liver injury.

Existing studies have demonstrated that overdose ethanol administration to mice can induce hepatic inflammation and ROS generation.[20] As an important ROS, HClO plays a variety of roles in the inflammation process, but the generation and distribution of this kind of ROS in the liver are blurred. So far, there has been no reliable tool to probe the HClO generation in the alcohol-induced liver injury process. We then sought to use our probe **TPA-ClO** to detect HClO production in the alcohol-induced liver injury process. Briefly, mice were intragastrically administered with 5 doses of 50% ethanol solution at intervals of 12 h to lead to acute liver injury. And **TPA-ClO** was used to detect the HClO production in liver tissues using a TPM. As shown in Fig. 4a and b, the liver tissues of the control mice fed with water exhibited a weak blue fluorescence and insignificant green fluorescence. When the mice were intragastrically administered with 50% ethanol solution (5 g kg^{-1} body weight), the liver tissues displayed a much higher ratio of green-to-blue fluorescence, indicating that there was a much higher level of HClO production in alcohol-induced liver injury tissues (Fig. 4c and d). As expected, when the mice were intragastrically fed with a higher dosage of 50% ethanol solution (10 g kg^{-1} body weight), a much brighter green fluorescence together with a further reduced blue fluorescence was observed, which can be ascribed to the worsened liver injury and accumulated HClO

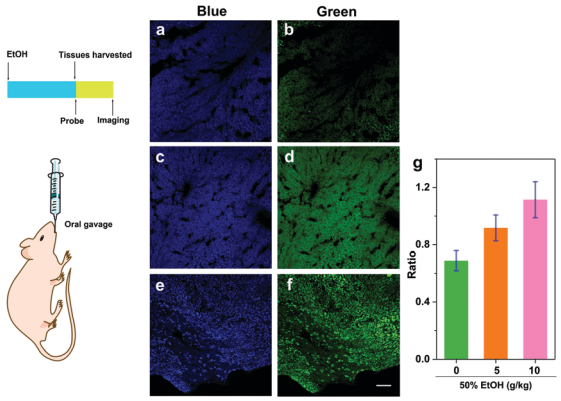

Fig. 4 Two-photon images of HClO production in the alcohol-induced liver injury process with **TPA-ClO**. Mice were fed with 5 doses of water (a and b) and 50% EtOH solution (5 g kg^{-1} body weight (c and d); 10 g kg^{-1} body weight (e and f)) by oral gavage at intervals of 12 h, respectively. Then, their liver tissues were harvested and incubated with 20 μM **TPA-ClO** for 0.5 h. (g) Fluorescence ratios for a–f. The TP excited fluorescence was collected in the blue channel (370–450 nm) and green channel (500–600 nm) upon excitation at 720 nm. Scale bar: 100 μm.

concentration (Fig. 4e and f). H&E staining results elucidated that the mice fed with 50% ethanol solution (10 g kg^{-1} body weight) had obviously higher degrees of liver injury than the other two groups (Fig. S10, ESI†), which agreed with the fluorescence imaging results. These results clearly revealed the production of HClO in the alcohol-induced liver injury process, and the concentration of HClO was dependent on alcohol dose in this process. By virtue of this probe **TPA-ClO**, the HClO production profile can be vividly monitored under a TPM for the first time. Besides, these results also implied that HClO may be an essential indicator of alcohol-induced liver injury. Although the functions of HClO in the liver injury process obviously need further investigations, our work suggests that the probe **TPA-ClO** may provide a competent tool for the study of HClO's roles in this pathological process and others.

In summary, a ratiometric two-photon fluorescent probe for detecting and imaging HClO was deliberately designed based on the oxidation of a thioanisole derivative by HClO. The probe afforded a ratiometric signal for the detection of HClO *in vitro* with high selectivity and sensitivity. The probe can enter into zebrafish and visualize the changes in the HClO level in the LPS-induced liver injury of the zebrafish *in vivo*. Furthermore, the probe was applied for imaging of HClO in liver tissues of mice, which revealed the generation profile of HClO in the alcohol-induced liver injury process for the first time. The probe may also provide a reliable tool for studying the distributions and functions of HClO in other biological and pathological events.

This work was financially supported by the National Natural Science Foundation of China (No. 21575109, 21625503, 21804033).

Conflicts of interest

There are no conflicts to declare.

Notes and references

1 H. K. Seitz, R. Bataller, H. Cortez-Pinto, B. Gao, A. Gual, C. Lackner, P. Mathurin, S. Mueller, G. Szabo and H. Tsukamoto, *Nat. Rev. Dis. Primers.*, 2018, **4**, 16.
2 J. P. Connor, P. S. Haber and W. D. Hall, *Lancet*, 2016, **387**, 988–998.
3 K. Wang, *Cell Death Dis.*, 2014, **5**, e996.
4 C. C. Winterbourn, *Nat. Chem. Biol.*, 2008, **4**, 278–286.
5 D. I. Pattison and M. J. Davies, *Biochemistry*, 2006, **45**, 8152–8162.
6 N. J. Mehta, K. Asmaro, D. J. Hermiz, M. M. Njus, A. H. Saleh, K. A. Beningo and D. Njus, *Free Radical Biol. Med.*, 2016, **101**, 44–52.
7 L. K. Stamp, I. Khalilova, J. M. Tarr, R. Senthilmohan, R. Turner, R. C. Haigh, P. G. Winyard and A. J. Kettle, *Rheumatology*, 2012, **51**, 1796–1803.
8 C. Gorrini, I. S. Harris and T. W. Mak, *Nat. Rev. Drug Discovery*, 2013, **12**, 931–947.
9 B. Pan, H. Ren, X. Lv, Y. Zhao, B. Yu, Y. He, Y. Ma, C. Niu, J. Kong, F. Yu, W. B. Sun, Y. Zhang, B. Willard and L. Zheng, *J. Transl. Med.*, 2012, **10**, 65.
10 (*a*) Y. Koide, Y. Urano, K. Hanaoka, T. Terai and T. Nagano, *J. Am. Chem. Soc.*, 2011, **133**, 5680–5682; (*b*) T. Li, L. Wang, S. Lin, X. Xu, M. Liu, S. Shen, Z. Yan and R. Mo, *Bioconjugate Chem.*, 2018, **29**, 2838–2845; (*c*) B. Zhu, P. Li, W. Shu, X. Wang, C. Liu, Y. Wang, Z. Wang, Y. Wang and B. Tang, *Anal. Chem.*, 2016, **88**, 12532–12538; (*d*) H. Ma, B. Song, Y. Wang, D. Cong, Y. Jiang and J. Yuan, *Chem. Sci.*, 2017, **8**, 150–159; (*e*) Y. Wu, J. Wang, F. Zeng, S. Huang, J. Huang, H. Xie, C. Yu and S. Wu, *ACS Appl. Mater. Interfaces*, 2016, **8**, 1511–1519; (*f*) Y. Hong, H. Wang, M. Xue, P. Zhang, W. Liu, S. Chen, R. Zeng, J. Cui, Y. Gao and J. Chen, *Mater. Chem. Front.*, 2019, **3**, 203–208; (*g*) P. Zhang, H. Wang, D. Zhang, R. Zeng, L. Xiao, H. Tao, Y. Long, P. Yi and J. Chen, *Sens. Actuators, B*, 2018, **255**, 2223–2231; (*h*) H. Wang, P. Zhang, Y. Hong, B. Zhang, P. Yi and J. Chen, *Polym. Chem.*, 2017, **8**, 5795–5802; (*i*) Y. Huang, P. Zhang, M. Gao, F. Zeng, A. Qin, S. Wu and B. Z. Tang, *Chem. Commun.*, 2016, **52**, 7288–7291; (*j*) Y. W. Jun, S. Sarkar, S. Singha, Y. J. Reo, H. R. Kim, J. J. Kim, Y. T. Chang and K. H. Ahn, *Chem. Commun.*, 2017, **53**, 10800–10803.
11 H. M. Kim and B. R. Cho, *Chem. Rev.*, 2015, **115**, 5014–5055.
12 (*a*) H. J. Kim, C. S. Lim, H. W. Lee, H. S. Lee, Y. J. Um, H. K. Han and H. M. Kim, *Biomaterials*, 2017, **41**, 251–259; (*b*) H. J. Choi, C. S. Lim, M. K. Cho, J. S. Kang, S. J. Park, S. M. Park and H. M. Kim, *Sens. Actuators, B*, 2019, **283**, 810–819; (*c*) Y. J. Kim, S. J. Park, C. S. Lim, D. J. Lee, C.-K. Noh, K. Lee, S. J. Shin and H. M. Kim, *Anal. Chem.*, 2019, **91**, 9246–9250.
13 P. Wei, X. Bi, Z. Wu and Z. Xu, *Org. Lett.*, 2005, **7**, 3199–3202.
14 (*a*) Q. Xu, C. H. Heo, G. Kim, H. W. Lee, H. M. Kim and J. Yoon, *Angew. Chem., Int. Ed.*, 2015, **54**, 4890–4894; (*b*) C. Duan, M. Won, P. Verwilst, J. Xu, H. S. Kim, L. Zeng and J. S. Kim, *Anal. Chem.*, 2019, **91**, 4172–4178.
15 H. Zhu, J. Fan, J. Du and X. Peng, *Acc. Chem. Res.*, 2016, **49**, 2115–2126.
16 J. J. Hu, N. K. Wong, M. Y. Lu, X. Chen, S. Ye, A. Q. Zhao, P. Gao, R. Y. T. Kao, J. Shen and D. Yang, *Chem. Sci.*, 2016, **7**, 2094–2099.
17 Y. Zhang, J. Cen, Z. Jia, C. D. Hsiao, Q. Xia, X. Wang, X. Chen, R. Wang, Z. Jiang, L. Zhang and K. Liu, *Antimicrob. Agents Chemother.*, 2019, **63**, e01639-18.
18 D. L. Howarth, C. Yin, K. Yeh and K. C. Sadler, *Zebrafish*, 2013, **10**, 199–210.
19 P. Zhang, H. Wang, Y. Hong, M. Yu, R. Zeng, Y. Long and J. Chen, *Biosens. Bioelectron.*, 2018, **99**, 318–324.
20 T. C. Tan, D. H. Crawford, L. A. Jaskowski, V. N. Subramaniam, A. D. Clouston, D. I. Crane, K. R. Bridle, G. J. Anderson and L. M. Fletcher, *Lab. Invest.*, 2013, **93**, 1295.